Congreso de Métodos Numéricos en Ingeniería 2009
Barcelona, 29 junio al 2 de julio 2009


# APPLICATION OF THE LOG-CONFORMATION TECHNIQUE TO 3D FREE SURFACE FLOWS

**M. F. Tomé[1*], A. Castelo[1*], A. M. Afonso[2*], F. T. Pinho[3*], M. A. Alves[2*]**

1: Departamento de Matemática Aplicada e Estatística
Instituto de Ciências Matemáticas e de Computação
Universidade de São Paulo
São Carlos - SP - Brasil
e-mail: {murilo, castelo}@icmc.usp.br

2: CEFT- Departamento de Engenharia Química
Faculdade de Engenharia da Universidade do Porto
Porto - Portugal
e-mail:{aafonso, mmalves}@fe.up.pt
3: CEFT- Departamento de Engenharia Mecânica e Gestão Industrial
Faculdade de Engenharia da Universidade do Porto
Porto - Portugal
e-mail: fpinho@fe.up.pt

**Key words:** Log-conformation tensor, Free surface flows, Finite difference, Extrudate swell

**Abstract.** *The numerical simulation of flows of very elastic fluids has been a subject of intense research for the past decades with important industrial applications. Therefore, it comes as no surprise that many efforts have been made to improve the convergence capabilities of the numerical methods used. Recently, an important contribution to the High Weissenberg Number Problem has been presented by Fattal and Kupferman [J. non-Newt. Fluid Mech. 123, 281-285, (2004)], who developed the matrix-logarithm of the conformation tensor technique, henceforth called log-conformation tensor. This methodology guarantees that solutions of viscoelastic flow problems are physically admissible and can deal with sharp elastic stress layers. Several investigators have been using the log-conformation tensor and results for high Weissenberg number flows have been reported. However, this technique has only been applied to simulate confined flows of viscoelastic fluids. In this work we investigate the application of the log-conformation tensor technique to three-dimensional unsteady free surface flows. We applied the log-conformation tensor formulation to solve the Oldroyd-B constitutive equation and solved the momentum equation using a finite difference Marker-and-Cell type method. Results for the simulation of the extrudate swell of Oldroyd-B fluids at high Weissenberg numbers are presented.*

## 1 INTRODUCTION

Free surface flows of complex fluids are important in the polymer processing industry, the typical application being the extrusion process of a polymer melt. In this process, a polymer melt is forced to flow through a die using a piston and the deformation of the polymer as it exits the die eventually determines the final shape of the extrudate. Hence, accurate simulation of the complex flow along the die and at the exit is extremely important in order to properly design the shape of the die that produces the extrudate with the desired prescribed shape [1]. After exiting the die the fluid usually swells to an extent that is strongly dependent on the fluid rheology and on the stress conditions, i.e., which depends on the flow history inside the die. For this reason, the inverse problem of finding the correct die shape that produces the desired extrudate profile [1] is of paramount importance in the polymer processing industry. On the other hand, increasing the production rate often leads to the onset of flow instabilities, and the surface of the extrudate looses the desired smoothness. This sharkskin instability arises at high flow rates, and at more extreme conditions melt fracture may occur. These instabilities are undesirable and have a negative impact on the quality of the produced extrudate [2]. Accurate modeling of the flow in these complex geometries can have a critical role in the optimization of the operational parameters, namely the productivity of the extrusion process.

In this work we study numerically the flow at the exit of a circular tube, known as the die-swell problem (or more accurately called extrudate swell), aiming at quantifying the swell ratio as a function of the Weissenberg number ($We$), for a fluid that is described by the Oldroyd-B model. Due to the discontinuity of the tube wall at the die exit, the stress and pressure fields are singular at the exit of the tube [3]. This singular behavior is difficult to model and typically the maximum Weissenberg number where convergence is achieved is modest, of the order of one for Oldroyd-type fluids. This inability to simulate viscoelastic flows at high We has been the major challenge in computational rheology for the last three decades [4] and is known as the High Weissenberg Number Problem (HWNP)[5]. Numerical simulation of different viscoelastic flows suggests that this breakdown in numerical stability is related to the emergence of large stress gradients. This may be related to the unsuitability of polynomial-based interpolation schemes, used to calculate stress profiles, to perform well in regions of high shear rates or near stagnation points where the stresses exhibit exponential growth [6] even leading to unphysical stress values. Recently, a remedy for the HWNP was proposed by Fattal and Kupferman [6], known as the log-conformation technique. According to this methodology, an evolution equation for the logarithm of the conformation tensor is solved, reducing the large gradients of the stress and conformation tensor fields and also eliminating the loss of positive definiteness of the conformation tensor. This new logarithm of the conformation tensor variable can be approximated numerically with better accuracy in problematic flow regions, where the stress field has an exponential behavior. In addition, the positive definiteness of the conformation tensor is garanteed no matter the accuracy of the computed solution for the

logarithm of the conformation tensor.

During the last five years several authors have implemented the log-conformation technique in their viscoelastic codes (e.g. Hulsen et al. [4]; Kwon [7]; Afonso et al. [8]). In all cases an enhancement of the stability of the numerical method was reported, demonstrating the advantage of the log-conformation tensor approach. In this work we describe the implementation of the log-conformation technique in a finite-difference method used to calculate free surface flows of viscoelastic fluids, and assess the impact upon the stability and accuracy of the numerical solutions obtained for the die swell benchmark flow of a viscoelastic fluid described by the Oldroyd-B constitutive equation.

The remainder of this paper is organised as follows: in Section 2 we present the basic equations and the log-conformation methodology; in Section 3 we briefly describe the numerical method and proceed to the presentation of the numerical results of the three-dimensional unsteady extrudate swell of an Oldroyd-B fluid; Section 5 ends the paper with a brief summary of our findings.

## 2 BASIC EQUATIONS

The governing equations for incompressible flows are the mass conservation equation and the equation of motion which, in nondimensional form, can be written as (see Tomé et al. [9])

$$\nabla \cdot \mathbf{u} = 0 \,, \tag{1}$$

$$\frac{\partial \mathbf{u}}{\partial t} + (\mathbf{u} \cdot \nabla)\mathbf{u} = -\nabla p + \frac{1}{Re}\frac{\lambda_2}{\lambda_1}\nabla^2 \mathbf{u} + \nabla \cdot \mathbf{S} + \frac{1}{Fr}\mathbf{g} \,. \tag{2}$$

The non-Newtonian modified stress tensor $\mathbf{S}$ is obtained by an appropriate constitutive law after employing the change of variables of the EVSS technique [10]. In this work the fluid is described by the Oldroyd-B model which leads to the following equation for the tensor $\mathbf{S}$ (see Tomé et al. [9])

$$\mathbf{S} + We\,\overset{\nabla}{\mathbf{S}} = \frac{2}{Re}\left(1 - \frac{\lambda_2}{\lambda_1}\right)\mathbf{D} \,. \tag{3}$$

In the equations above, $t$ is the time, $\mathbf{u}$ is the velocity vector, $p$ is the pressure, $\mathbf{g}$ is the gravitational field, $\lambda_1$ and $\lambda_2$ are the relaxation and retardation times, respectively, $\mathbf{S}$ is the non-Newtonian modified stress tensor and $\mathbf{D} = \frac{1}{2}((\nabla \mathbf{u}) + (\nabla \mathbf{u})^{\mathrm{T}})$ is the rate of deformation tensor. The nondimensional numbers $Re, Fr, We$ are, respectively, the Reynolds, Froude and Weissenberg numbers given by

$$Re = \frac{\rho\, U\, L}{\eta_0} \,; \quad Fr = \frac{U}{\sqrt{gL}} \qquad We = \lambda_1 \frac{U}{L} \,,$$

where $L$ and $U$ are length and velocity scales for normalization to be defined later when describing the flow geometry. The symbol $\overset{\nabla}{(\cdot)}$ represents the upper convected derivative

defined by

$$\overset{\nabla}{\boldsymbol{\phi}} = \frac{\partial \boldsymbol{\phi}}{\partial t} + (\mathbf{u}\cdot\nabla)\boldsymbol{\phi} - (\nabla\mathbf{u})^{\mathrm{T}}\boldsymbol{\phi} - \boldsymbol{\phi}\,(\nabla\mathbf{u})\,. \tag{4}$$

Alternatively, the constitutive law (3) can be formulated in terms of the conformation tensor $\mathbf{A}$,

$$\mathbf{S} = \frac{1}{Re\,We}\left(1 - \frac{\lambda_2}{\lambda_1}\right)(\mathbf{A} - \mathbf{I}) \tag{5}$$

where $\mathbf{I}$ is the unitary tensor. The conformation tensor $\mathbf{A}$ is obtained by an appropriate evolution equation, which for the Oldroyd-B model is given by

$$\frac{\partial \mathbf{A}}{\partial t} + (\mathbf{u}\cdot\nabla)\mathbf{A} - (\nabla\mathbf{u})^{\mathrm{T}}\,\mathbf{A} - \mathbf{A}\,(\nabla\mathbf{u}) = \frac{1}{We}(\mathbf{I} - \mathbf{A}) \tag{6}$$

To solve (6) we decompose the velocity gradient as (see [6]):

$$\nabla\mathbf{u} = \boldsymbol{\Omega} + \mathbf{B} + \mathbf{N}\mathbf{A}^{-1} \tag{7}$$

where the tensors $\boldsymbol{\Omega}$ and $\mathbf{N}$ are anti-symmetric and the tensor $\mathbf{B}$ is symmetric, traceless and commutes with $\mathbf{A}$. The tensor $\mathbf{B}$ generates a pure (area preserving) extension while $\boldsymbol{\Omega}$ is responsible for rotations. Substituting the decomposition (7) into equation (6), one finds that the term $\mathbf{N}\mathbf{A}^{-1}$ cancels by anti-symmetry and the following transformed equation for the conformation tensor (see [6]) is obtained

$$\frac{\partial \mathbf{A}}{\partial t} + (\mathbf{u}\cdot\nabla)\mathbf{A} - (\boldsymbol{\Omega}\mathbf{A} - \mathbf{A}\boldsymbol{\Omega}) - 2\mathbf{B}\mathbf{A} = \frac{1}{We}(\mathbf{I} - \mathbf{A})\,. \tag{8}$$

### 2.1 The LOG-conformation representation

The LOG-conformation representation can be obtained by replacing equation (8) with an equivalent equation for the tensor

$$\boldsymbol{\Psi} = \log(\mathbf{A})\,. \tag{9}$$

A symmetric Positive definite (SPD) matrix can always be diagonalized so we can find a matrix $\mathbf{R}$ and a diagonal matrix $\boldsymbol{\Lambda}$ so that $\mathbf{A} = \mathbf{R}\boldsymbol{\Lambda}\mathbf{R}^{\mathrm{T}}$. Matrix $\mathbf{R}$ is an orthogonal matrix formed by the three eigenvectors of $\mathbf{A}$, whereas the corresponding eigenvalues form the diagonal matrix $\boldsymbol{\Lambda}$. Thus, $\log(\mathbf{A}) = \mathbf{R}\,\log(\boldsymbol{\Lambda})\,\mathbf{R}^{\mathrm{T}}$. The transformation from equation (8) to an equation for $\boldsymbol{\Psi} = \log(\mathbf{A})$ is straightforward (see [6] for details) and leads to

$$\frac{\partial \boldsymbol{\Psi}}{\partial t} + (\mathbf{u}\cdot\nabla)\boldsymbol{\Psi} - (\boldsymbol{\Omega}\boldsymbol{\Psi} - \boldsymbol{\Psi}\boldsymbol{\Omega}) - 2\mathbf{B} = \frac{1}{We}(\mathbf{e}^{-\boldsymbol{\Psi}} - \mathbf{I})\,. \tag{10}$$

The gist of this transformation is an appropriate decomposition of the velocity gradient into extensional and rotational components. Details of the equations involved in this decomposition are given in [6]. The rotational component operates on $\log(\mathbf{A})$ in the same way as it operates on $\mathbf{A}$; the extensional component operates on $\log(\mathbf{A})$ additively.

Therefore, we need to solve equations (1), (2) and (5) together with equations (9) and (10) for the unknowns $\mathbf{u}$, $p$, $\mathbf{S}$, $\mathbf{A}$ and $\boldsymbol{\Psi}$, respectively.

### 2.2 Boundary Conditions

In order to solve equations (1) and (2) it is necessary to impose boundary conditions for the velocity field on mesh boundaries. For rigid boundaries we employ the no-slip condition $\mathbf{u} = \mathbf{0}$ while at fluid entrances (inflows) the normal velocity is specified by $U_n = U_{in}$ and the tangential velocities are set to zero, namely, $U_{m1} = U_{m2} = 0$, where $m_1$ and $m_2$ denote tangential directions to the inflow plane. At fluid exits (outflows) the Neumann condition $\frac{\partial \mathbf{u}}{\partial n} = 0$ is adopted. We consider a viscous fluid flowing in a passive atmosphere and surface tension forces are neglected at the liquid-gas interface. Then, on the liquid free surface the correct boundary conditions are given by (see Batchelor [11], page 153)

$$\mathbf{n} \cdot (\boldsymbol{\sigma} \cdot \mathbf{n}) = 0 \ , \tag{11}$$

$$\mathbf{m1} \cdot (\boldsymbol{\sigma} \cdot \mathbf{n}) = 0 \ , \tag{12}$$

$$\mathbf{m2} \cdot (\boldsymbol{\sigma} \cdot \mathbf{n}) = 0 \ , \tag{13}$$

where $\mathbf{n}$ is the outward unit normal vector to the free surface and $\mathbf{m1}, \mathbf{m2}$ are unit tangential vectors and $\boldsymbol{\sigma}$ is the total stress tensor $\boldsymbol{\sigma} = -p\mathbf{I} + \frac{2}{Re}\left(\frac{\lambda_2}{\lambda_1}\right)\mathbf{D} + \mathbf{S}$.

## 3 NUMERICAL METHOD

The method of solution is based on the projection method introduced by Chorin [12] (for projection methods used within a finite element framework see Guermod and Quartapelle [14]).

To solve equations (1), (2), (10), (9) and (5) together with the equations defining the boundary conditions we use the methodology employed by Tomé et al. [9] for three-dimensional viscoelastic free surface flows governed by the Oldroyd-B model.

Suppose that $\mathbf{u}(\mathbf{x}, t_n)$, $\mathbf{S}(\mathbf{x}, t_n)$ are known and boundary conditions for velocity and pressure are given. Then, $\mathbf{u}(\mathbf{x}, t_{n+1})$, $p(\mathbf{x}, t_{n+1})$, $\boldsymbol{\Psi}(\mathbf{x}, t_{n+1})$, $\mathbf{A}(\mathbf{x}, t_{n+1})$ and $\mathbf{S}(\mathbf{x}, t_{n+1})$, where $t_{n+1} = t_n + \delta t$, can be obtained as follows:

**Step 1**: Let $\widetilde{p}(\mathbf{x}, t_n)$ be a pressure field which satisfies the correct pressure condition on the free surface. This pressure field is computed so that the normal stress condition (11) is satisfied.

**Step 2**: Compute the intermediate velocity field, $\widetilde{\mathbf{u}}(\mathbf{x}, t_{n+1})$:

$$\frac{\partial \widetilde{\mathbf{u}}}{\partial t} = -(\mathbf{u} \cdot \nabla)\mathbf{u} - \nabla \widetilde{p} + \frac{1}{Re}\left(\frac{\lambda_2}{\lambda_1}\right)\nabla^2 \mathbf{u} + \nabla \cdot \mathbf{S} + \frac{1}{Fr^2}\mathbf{g} \ , \tag{14}$$

with $\widetilde{\mathbf{u}}(\mathbf{x}, t_n) = \mathbf{u}(\mathbf{x}, t_n)$ using the correct boundary conditions for $\mathbf{u}(\mathbf{x}, t_n)$. These equations are solved by a finite difference method which is handled explicitly in time.

**Step 3**: Solve the Poisson equation

$$\nabla^2 \boldsymbol{\psi}(\mathbf{x}, t_{n+1}) = \nabla \cdot \widetilde{\mathbf{u}}(\mathbf{x}, t_{n+1}) \ . \tag{15}$$

The appropriate boundary conditions for this equation are [15]

$$\frac{\partial \psi}{\partial n} = 0 \text{ on rigid boundaries and } \psi = 0 \text{ on the free surface.}$$

**Step 4**: Compute the final velocity field to obey continuity

$$\mathbf{u}(\mathbf{x}, t_{n+1}) = \widetilde{\mathbf{u}}(\mathbf{x}, t_{n+1}) - \nabla \psi(\mathbf{x}, t_{n+1}). \tag{16}$$

**Step 5**: Compute the pressure field

$$p(\mathbf{x}, t_{n+1}) = \widetilde{p}(\mathbf{x}, t_n) + \frac{\psi(\mathbf{x}, t_{n+1})}{\delta t}. \tag{17}$$

**Step 6**: Decompose the velocity gradient as: $\nabla \mathbf{u}(\mathbf{x}, t_{n+1}) = \boldsymbol{\Omega} + \mathbf{B} + \mathbf{N}\mathbf{A}^{-1}$.

**Step 7**: Using $\mathbf{S}(\mathbf{x}, t_n)$ calculate the conformation tensor $\mathbf{A}(\mathbf{x}, t_n)$ from

$$\mathbf{A}(\mathbf{x}, t_n) = Re\, We \left( \frac{\lambda_1}{\lambda_1 - \lambda_2} \right) \mathbf{S}(\mathbf{x}, t_n) + \mathbf{I} \tag{18}$$

**Step 8**: Calculate matrices $\mathbf{R}^n$ and $\boldsymbol{\Lambda}^n$ such that $\mathbf{A}(\mathbf{x}, t_n) = \mathbf{R}^n \, \boldsymbol{\Lambda}^n \, (\mathbf{R}^n)^{\mathrm{T}}$ and then compute $\boldsymbol{\Psi}(\mathbf{x}, t_n) = \log(\mathbf{A}(\mathbf{x}, t_n)) = \mathbf{R}^n \, \log(\boldsymbol{\Lambda}) \, (\mathbf{R}^n)^{\mathrm{T}}$ and $\mathbf{e}^{-\boldsymbol{\Psi}(\mathbf{x}, \boldsymbol{t_n})} = (\mathbf{R}^n)^{\mathrm{T}} \, (\boldsymbol{\Lambda}^n)^{-1} \, \mathbf{R}^n$.

**Step 9**: Calculate $\boldsymbol{\Psi}(\mathbf{x}, t_{n+1})$ from

$$\begin{aligned} \boldsymbol{\Psi}(\mathbf{x}, t_{n+1}) = & \boldsymbol{\Psi}(\mathbf{x}, t_n) + \delta t \Big\{ - (\mathbf{u}(\mathbf{x}, t_{n+1}) \cdot \nabla) \boldsymbol{\Psi}(\mathbf{x}, t_n) \\ & + \left[ \boldsymbol{\Omega} \boldsymbol{\Psi}(\mathbf{x}, t_n) - \boldsymbol{\Psi}(\mathbf{x}, t_n) \boldsymbol{\Omega} \right] + 2\mathbf{B} + \frac{1}{We} (\mathbf{e}^{-\boldsymbol{\Psi}(\mathbf{x}, t_n)} - \mathbf{I}) \Big\} \end{aligned} \tag{19}$$

**Step 10**: Calculate matrices $\mathbf{R}^{(n+1)}$ and $\boldsymbol{\Lambda}^{(n+1)}$ such that

$$\boldsymbol{\Psi}(\mathbf{x}, t_{n+1}) = \mathbf{R}^{(n+1)} \, \boldsymbol{\Lambda}^{(n+1)} \, (\mathbf{R}^{(n+1)})^{\mathrm{T}} \tag{20}$$

**Step 11**: The conformation tensor $\mathbf{A}(\mathbf{x}, t_{n+1})$ is calculated by

$$\mathbf{A}(\mathbf{x}, t_{n+1}) = \mathbf{e}^{\boldsymbol{\Psi}(\mathbf{x}, t_{n+1})} = \mathbf{R}^{(n+1)} \, \mathbf{e}^{\boldsymbol{\Lambda}^{(n+1)}} \, (\mathbf{R}^{(n+1)})^{\mathrm{T}} \tag{21}$$

**Step 12**: Finally, the modified stress tensor $\mathbf{S}(\mathbf{x}, t_{n+1})$ is obtained from

$$\mathbf{S}(\mathbf{x}, t_{n+1}) = \frac{1}{Re\,We}\left(1 - \frac{\lambda_2}{\lambda_1}\right)\Big[\mathbf{A}(\mathbf{x}, t_{n+1}) - \mathbf{I}\Big] \tag{22}$$

**Step 13**: Update the positions of the marker particles. The last step in the calculation is to move the markers to their new positions by solving the pure advective differential equation

$$\frac{d\mathbf{x}}{dt} = \mathbf{u}(\mathbf{x}, t_{n+1}) \ , \tag{23}$$

for each particle. The fluid surface is defined by piecewise linear surfaces composed of triangular and quadrilateral shapes with these marker particles at their vertices. Details of particle movement are given in Tomé et al. [16].

### 3.1 Finite difference solution

We consider three-dimensional free surface flows and solve the equations above by the finite difference method on a staggered grid (see figure 1a). In order to follow the moving free surface a scheme to define the cells within the mesh is employed. The cells within the mesh are of different type: empty cells (E or blank cells in Figure 1b) (cells that do not contain fluid), full cells (F) (cells that contain fluid and are not in contact with empty cells), surface cells (S) (cells that contain fluid and necessarily share one or more faces with empty cells), inflow cells (I) (cells that define an inflow boundary), outflow cells (O) (cells that define an outflow boundary) and boundary cells (B) (cells that define a rigid boundary). Figure 1b illustrates the type of cells within the mesh for the 2D case.

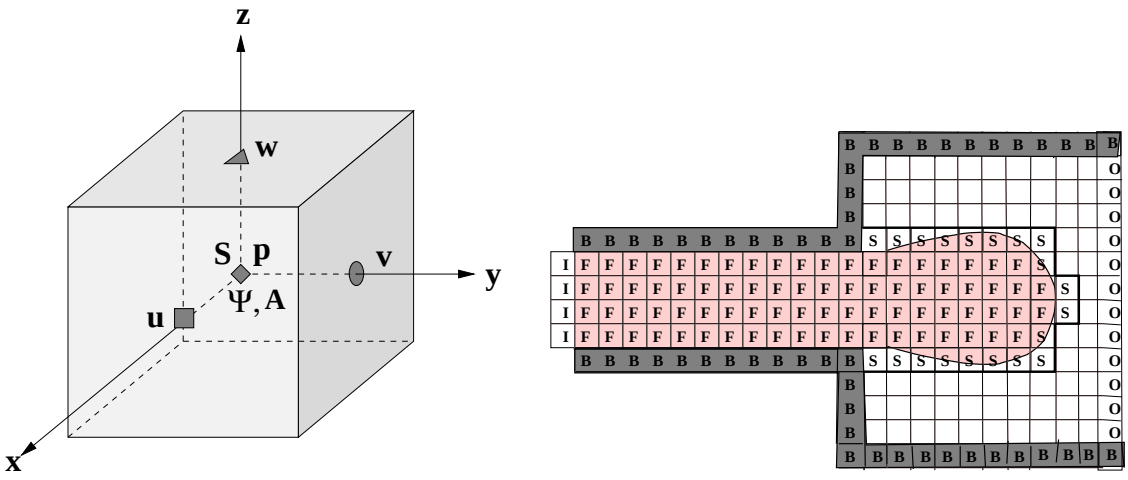


Figure 1: (a) Three-dimensional staggered grid used; (b) Types of cells within the mesh (Empty cells are empty).

The finite difference equations corresponding to **Step 1** to **Step 5** can be found in Tomé et al. [9] and so they are not presented here. The left hand side of the Poisson equation (15) is approximated by the Laplacian operator and is applied at every full cell in the domain. This originates a SPD linear system which is solved by the conjugate gradient method subject to a tolerance EPS of $10^{-10}$. **Step 6** to **Step 8** and **Step 10** to **Step 12** contain only products of matrices which are easily computed. The calculation of $\mathbf{\Psi}$ in **Step 9** is easily performed using finite differences, with the value of $\mathbf{\Psi}$ at cell faces coming from the convective term $(\mathbf{u}(\mathbf{x}, t_{n+1}) \cdot \nabla)\mathbf{\Psi}(\mathbf{x}, t_n)$ in equation (19) approximated by the high order CUBISTA method developed by Alves et al. [17].

## 4 NUMERICAL SIMULATION OF THREE-DIMENSIONAL UNSTEADY EXTRUDATE SWELL

The numerical method using the LOG-conformation technique described above has been embodied into a computer code which was applied to simulate the transient three dimensional extrudate swell.

We considered the flow produced by a jet as it emerges from a tube flowing into the air. This problem has practical industrial applications and has been studied both experimentally and numerically by many authors. For example, Tanner [18] presented a theory based on the K-BKZ constitutive model for obtaining swelling ratios while various authors have numerically investigated extrudate swell using the Oldroyd-B model, see for example Crochet and Keunings [19], Clermont and Normandin [13], Cormenzana et al. [20], Ngamaramvaranggul and Webster [23], to mention only a few.

To simulate this problem with the LOG-conformation tensor technique we employed the domain shown in Figure 2. We considered an empty pipe where at the pipe entrance (yellow surface shown in Figure 2) we imposed a fully developed velocity profile given by

$$w(x, y) = 2\left[R^2 - x^2 - y^2)\right], \qquad u = v = 0 \ . \tag{24}$$

On the fluid free surface the full free surface stress conditions (see equations (11)-(13)) were applied (for details see Tomé et al. [9]), while on the pipe walls the velocity obeyed the no-slip condition. At the outflow (pink surface shown in figure 2) the homogeneous Neumann conditions were applied.

To verify the correctness of the LOG-conformation code we simulated first the extrudate swell problem with the data employed by the EXPLICIT-Oldroyd-B model simulations of Tomé et al. [9] (see Table 1) and using an identical mesh. The time constants in the Oldroyd-B model were taken to be $\lambda_1 = 1$s and $\lambda_2 = 0.5$s so that in this simulation we had $We = \lambda_1 \frac{U}{R} = 1$ and $Re = \frac{\rho U R}{\eta_0} = 1$. We ran both the LOG-conformation and EXPLICIT-Oldroyd-B codes and compared the LOG-conformation results with those obtained by the explicit Oldroyd-B 3D technique. Figure 3 displays the results of both methods at times $t = 10s, 16s, 21$s while Figure 4 allows a quantitative comparision of

the swells obtained by both techniques. We can observe in Figure 3 that qualitatively the two flows are similar although the jet produced by the LOG-conformation technique reaches the outflow earlier than the jet from the EXPLICIT Oldroyd-B. This is confirmed in Figure 4 where we can see that the swell produced by the EXPLICIT method is slightly larger than the swell obtained with the LOG-conformation technique. These results show that the implementation of the LOG-conformation technique may be correct.

To demonstrate that the LOG-conformation method can cope with highly elastic fluids we performed three simulations of the time-dependent extrudate swell for increasing values of the Weissenberg number. Again we used the input data displayed in Table 1 and set the value of the time constant $\lambda_1$ to 0.5s, 1.0s and 1.5s which lead $We = 0.5, 1.0$ and 1.5, respectively. The ratio $\lambda_2/\lambda_1$ was kept constant and equal to 0.2 in all of these simulations. The results obtained with $We = 0.5, 1.0, 1.5$ are displayed in 3D in Figure 5 and in 2D in Figure 6. Figure 5 displays the dynamics of the jets flowing inside the pipe and then being extruded into the air. At times $t \leq 4.0$s the flow is still inside the pipe and there are no noticeable differences. For $t \geq 8.0$s all jets exited the pipe and flow into the atmosphere. At a later time of $t = 45.0$s we observe that all jets have reached the outflow boundary.

Looking at Figure 6 we can see better the sequence of events and especially the role of viscoelasticity. The jet having the smaller $We = 0.5$ flows faster than the others because of the lower swelling ratio and of continuity. The swelling ratios ($S_r = R_{max}/R$) obtained are shown in Table 2 where we can see that the variation of $S_r$ with $We$ is non-linear.

These results show that the LOG-conformation technique can indeed simulate flows of highly elastic fluids and it is important to mention that we were able to obtain converged solutions with $We = 1.5$, whereas with the explicit calculation method we only attained 1.2.

Table 1: Input data used for the simulation of the extrudate swell

| $h$(meshspacing) | $R$ | $U$ | $\eta_0$ | $\rho$ | EPS |
|---|---|---|---|---|---|
| 0.125 | 1.0 | 1.0 | 1.0 | 1.0 | $10^{-10}$ |

Table 2: Numerical simulation of time-dependent extrudate swell: $S_r$ obtained for various values of $We$.

| | $We = 0.0$ | $We = 0.5$ | $We = 1.0$ | $We = 1.5$ |
|---|---|---|---|---|
| $S_r$ | 1.0914 | 1.5111 | 1.8111 | 2.1889 |

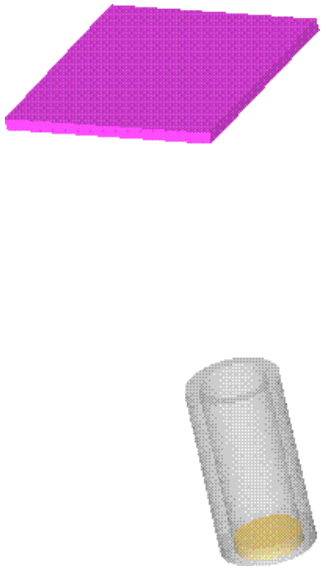

Figure 2: Domain used for the simulation of the transient extrudate swell. The yellow surface represents the pipe entrance, where an inflow boundary is defined, while the pink surface represents the region where an outflow boundary was set. The grey surface represents the pipe wall.

## CONCLUDING REMARKS

This paper dealt with the application of the LOG-conformation tensor technique to three-dimensional free surface flows governed by the Oldroyd-B constitutive equation. The basic equations arising from the LOG-conformation transformation were derived and implemented into a three-dimensional computer code. The momentum equations were solved by the finite difference method presented by Tomé et al. [9]. The LOG-conformation equation was also approximated by the finite difference method on a staggered grid and implemented into the Freeflow3D code of Castelo et al. [24]. The resulting code was applied to simulate the time-dependent extrudate swell of Oldroyd-B fluids and results were obtained for Weissenberg numbers 0.5, 1.0 and 1.5 and compared with corresponding predictions with the method of Tomé et al. [9], which does not rely on the LOG-conformation. Qualitatively the results for both methods were identical but the LOG-conformation technique resulted in slightly lower levels of swell. However, using the LOG-conformation we were able to obtain converged solutions up to $We$ numbers that were not possible without this technique. The results showed that the LOG-conformation technique can indeed cope with free surface flows of high elastic fluids.

## ACKNOWLEDGEMENTS

We gratefully acknowledge the support from the Brazilian funding agencies: FAPESP - Fundação de Amparo a pesquisa do Estado de São Paulo (grant No. $04/16064-9$) and CNPq - Conselho Nacional de Desenvolvimento Científico e Tecnológico (grants

a) LOG-CONFORMATION METHOD

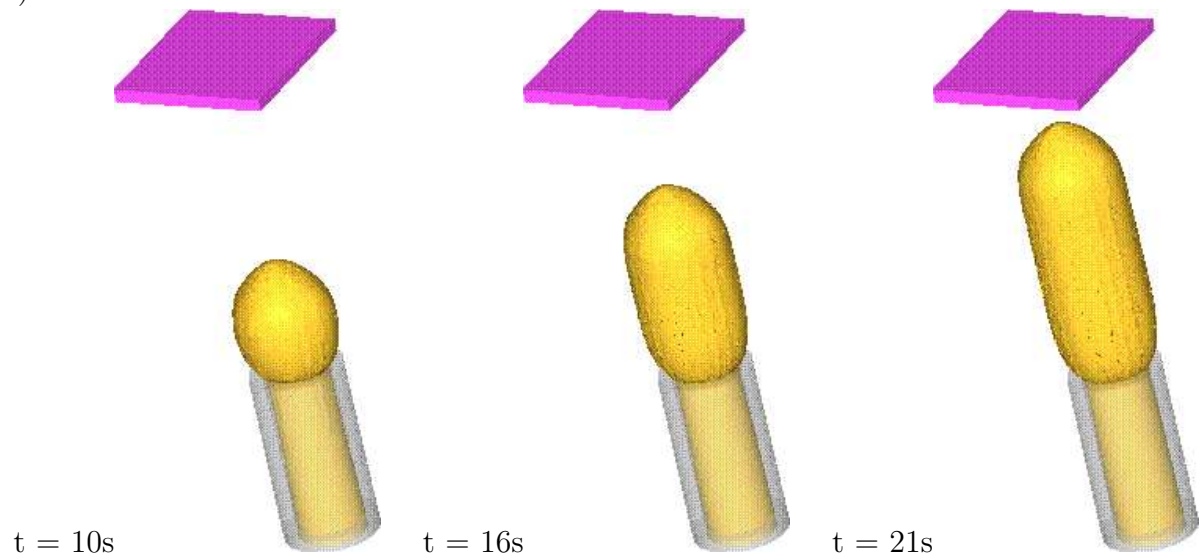


b) EXPLICIT METHOD

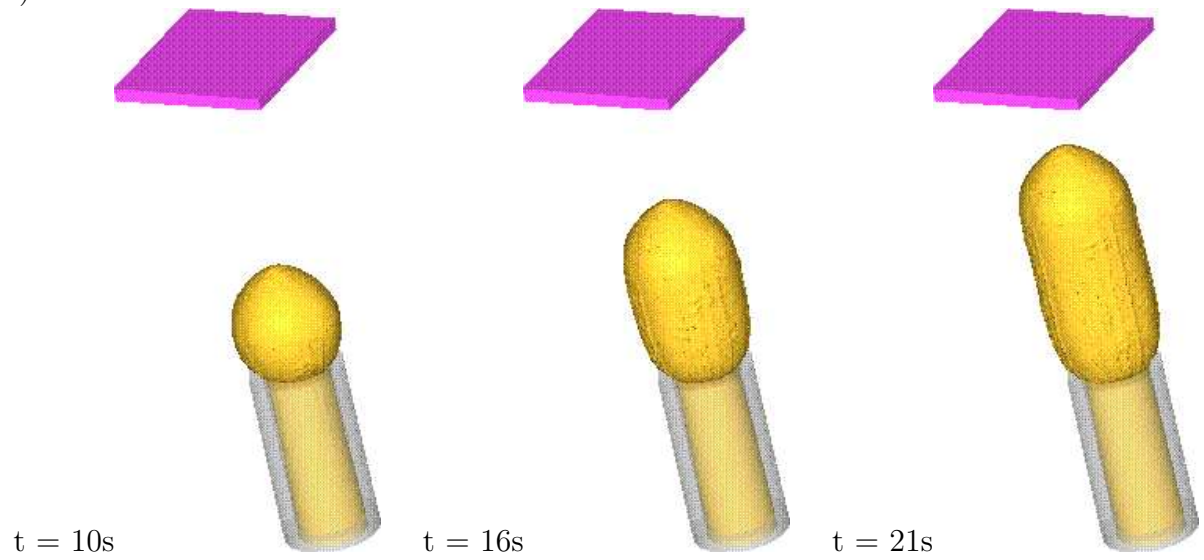


Figure 3: Numerical simulation of extrudate swell at different times - $Re = 1$, $We = 1$, $\lambda_2/\lambda_1 = 0.5$. a) LOG-conformation technique presented in this paper; b) Explicit method of Tomé et al. [9].

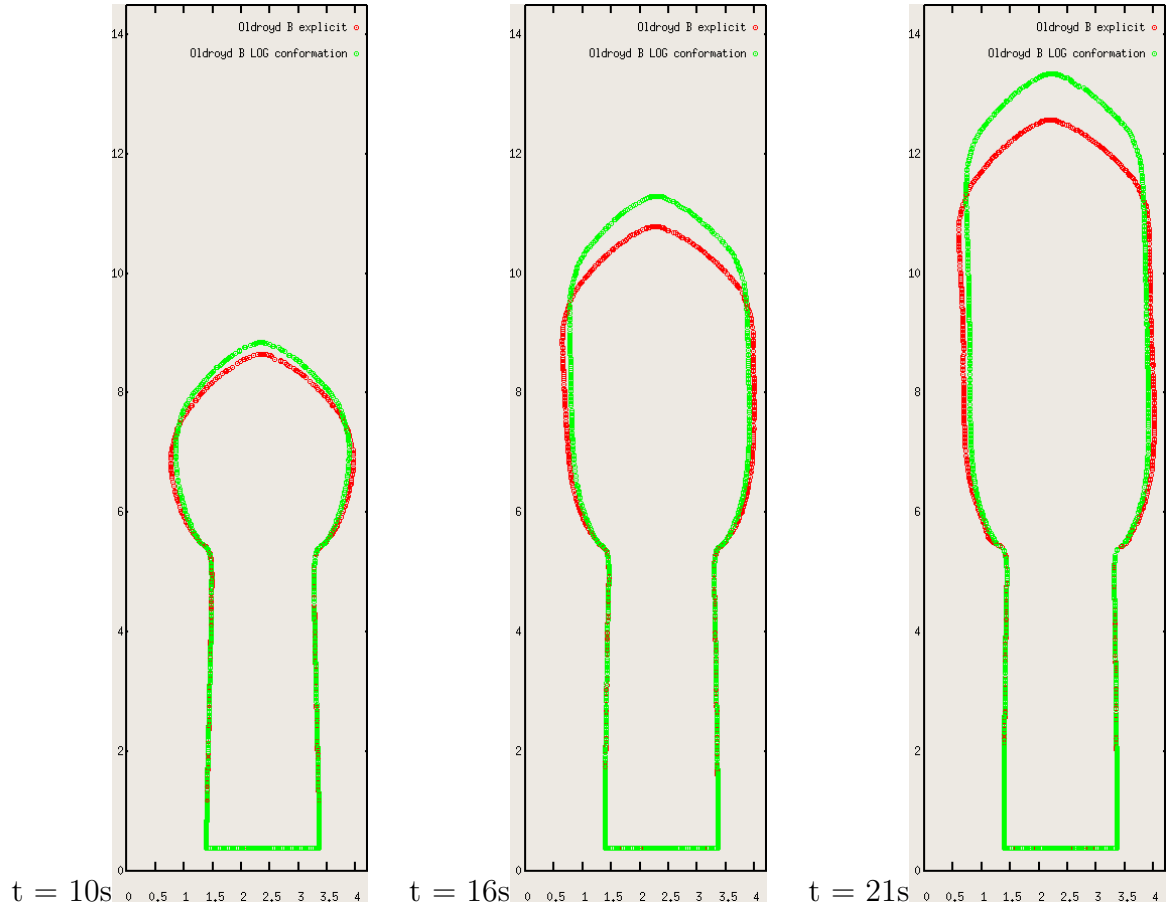


Figure 4: Numerical simulation of extrudate swell at different times. Comparison between the swells obtained by the explicit method of Tomé et al. [9] and the LOG-conformation technique.

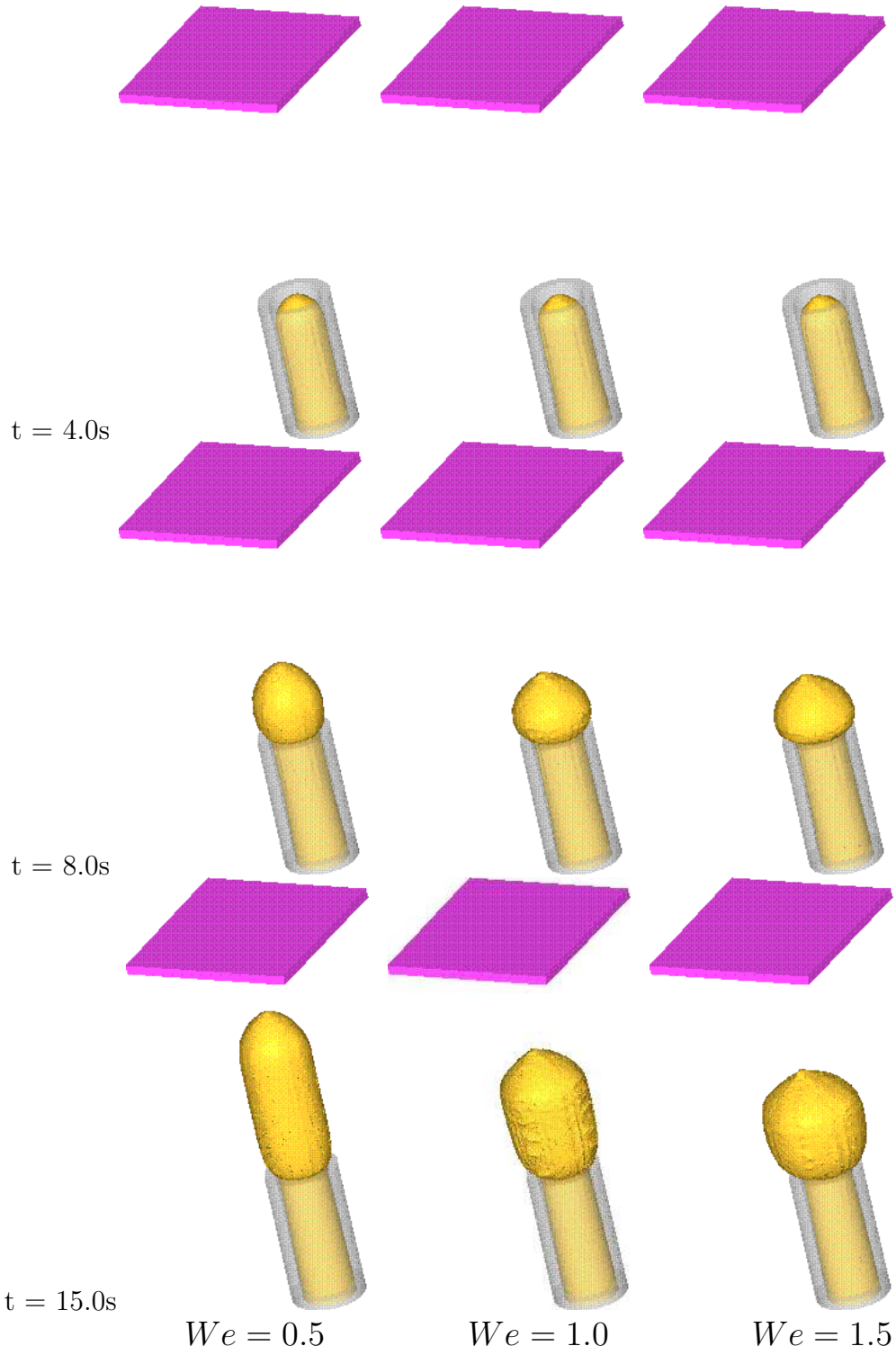


Figure 5: Numerical simulation of three-dimensional unsteady extrudate swell using the LOG-conformation technique. $Re = 1$. Flow visualization at different times.

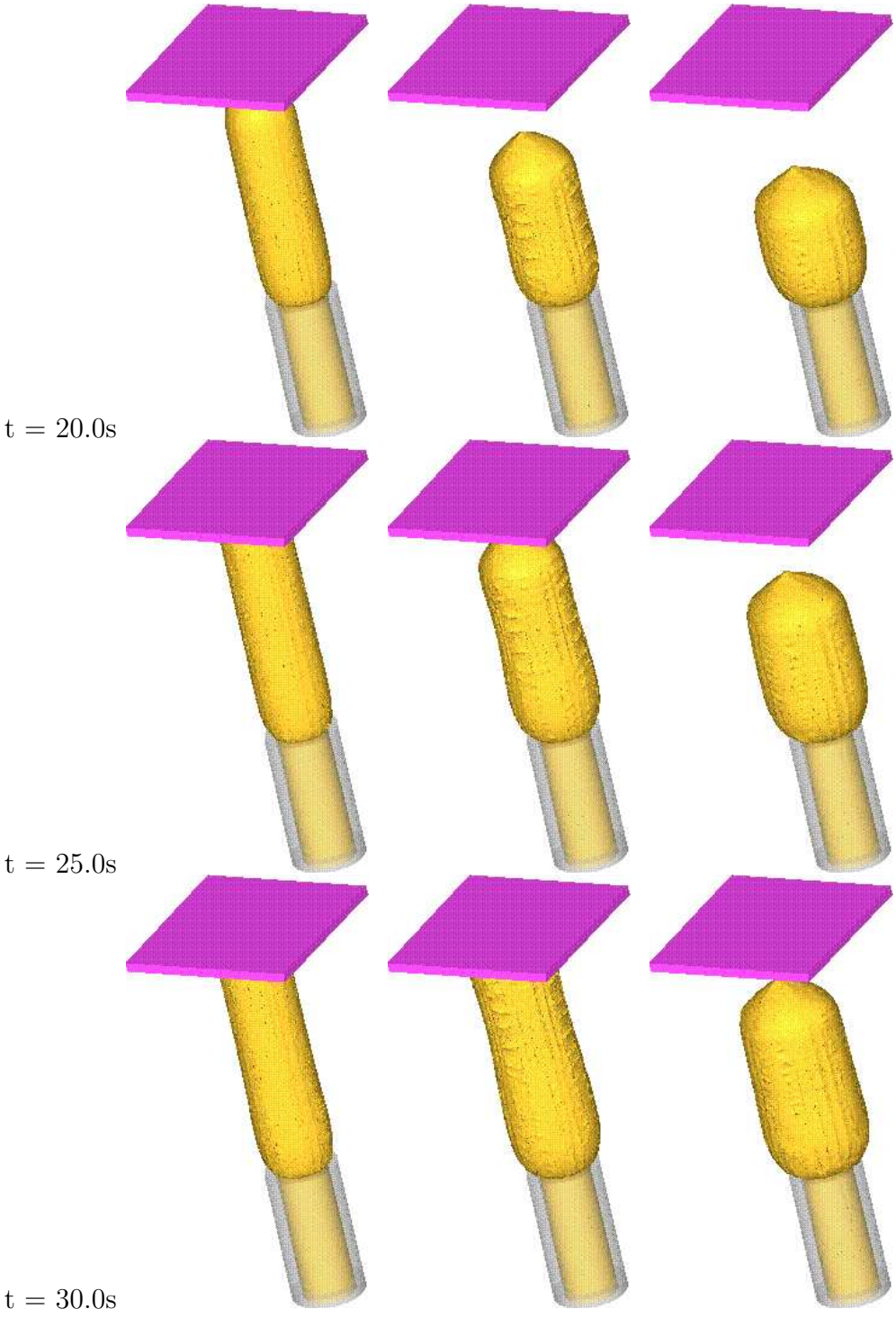


Figure 5. Continued.

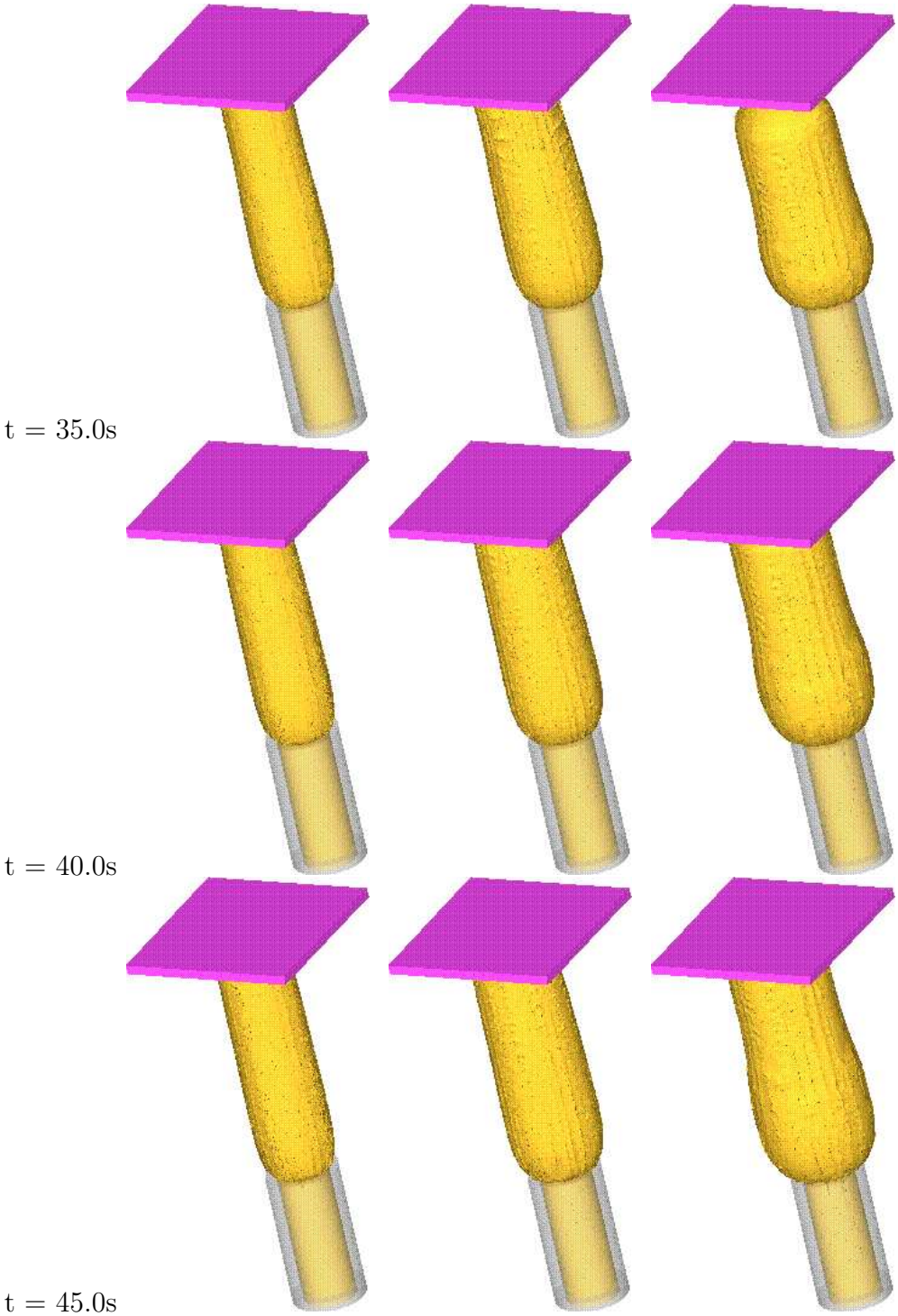


Figure 5. Continued.

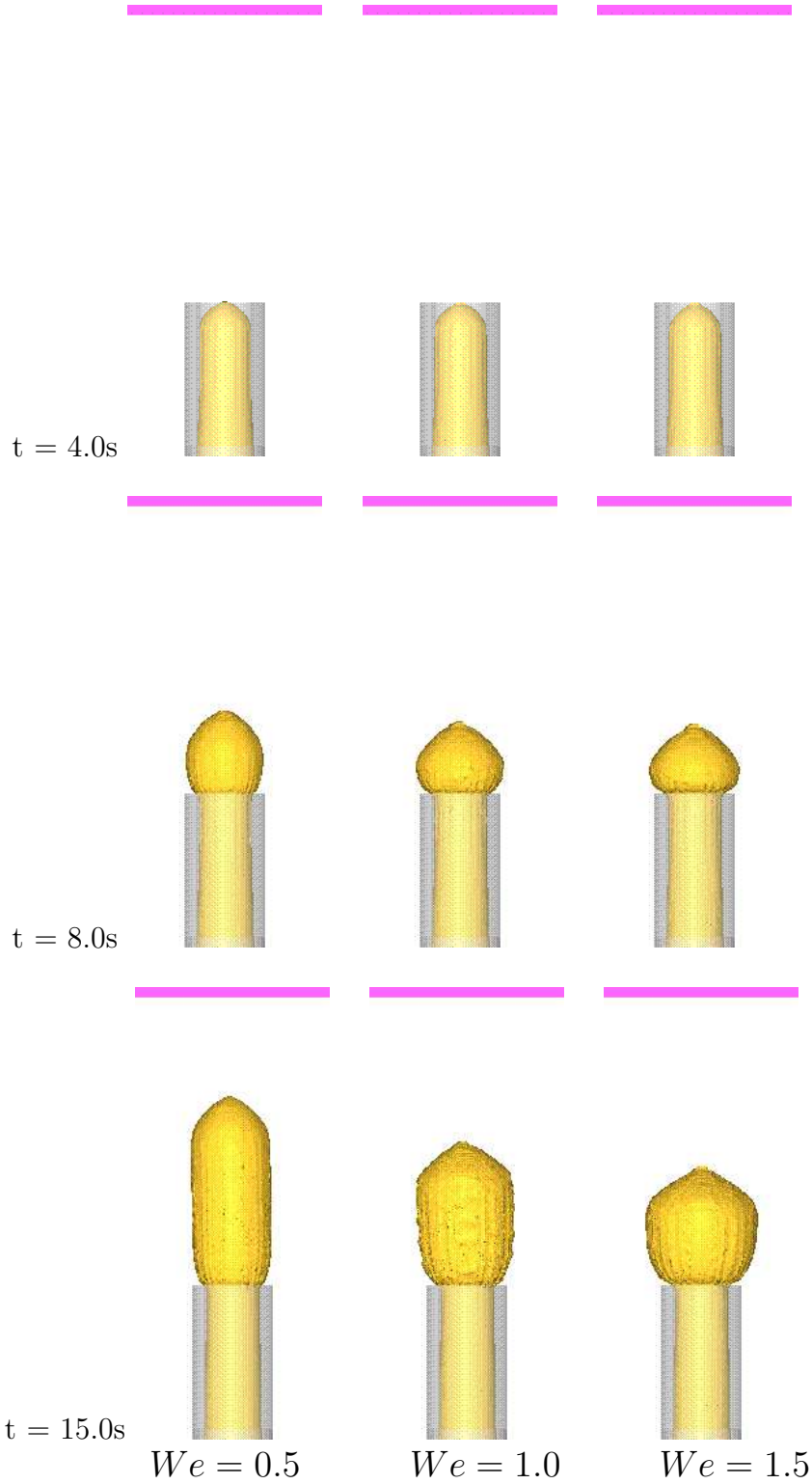


Figure 6: Numerical simulation of unsteady extrudate swell using the LOG-conformation technique. $Re = 1$. Front view visualization at different times.

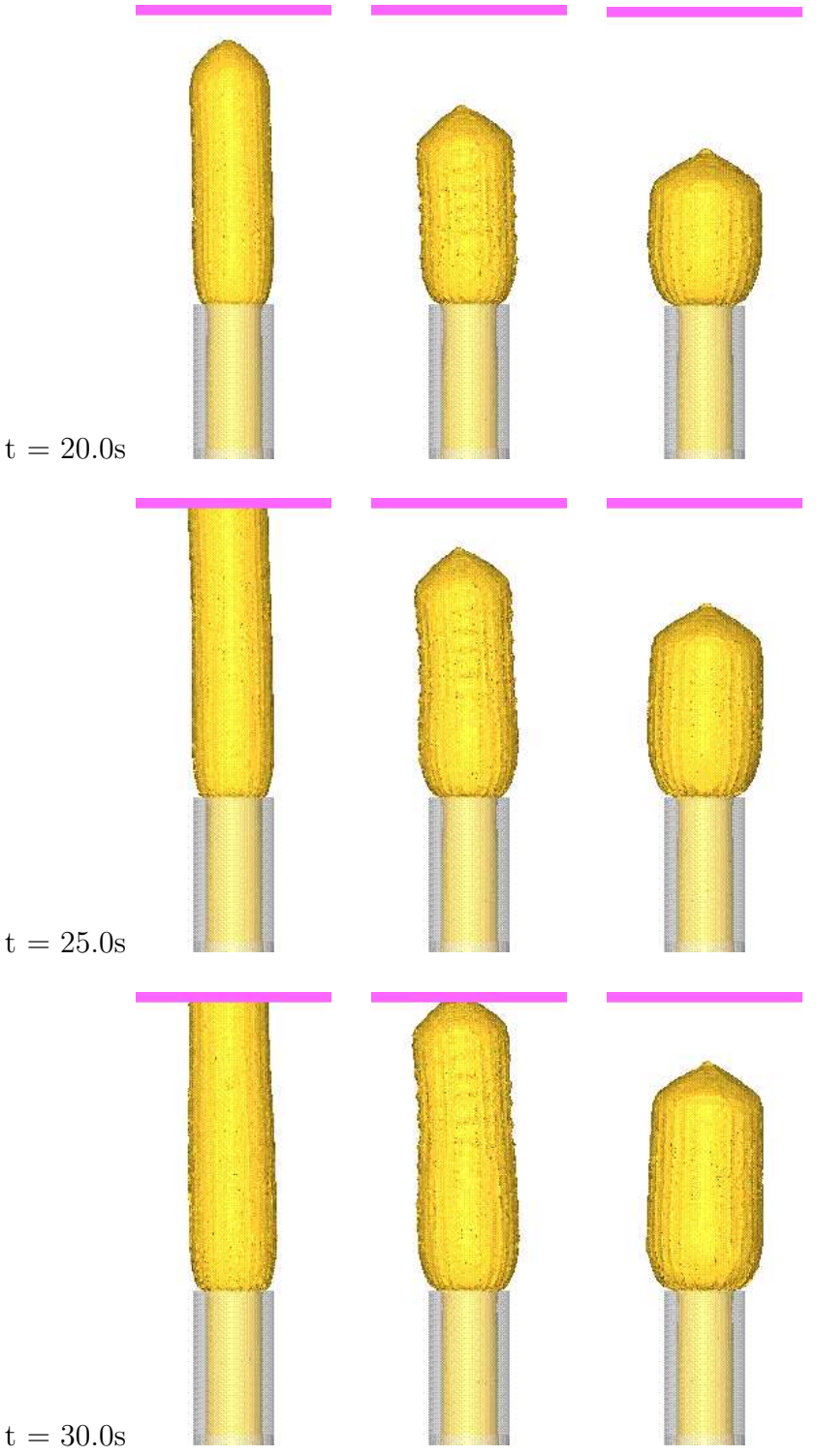


Figure 6. Continued.

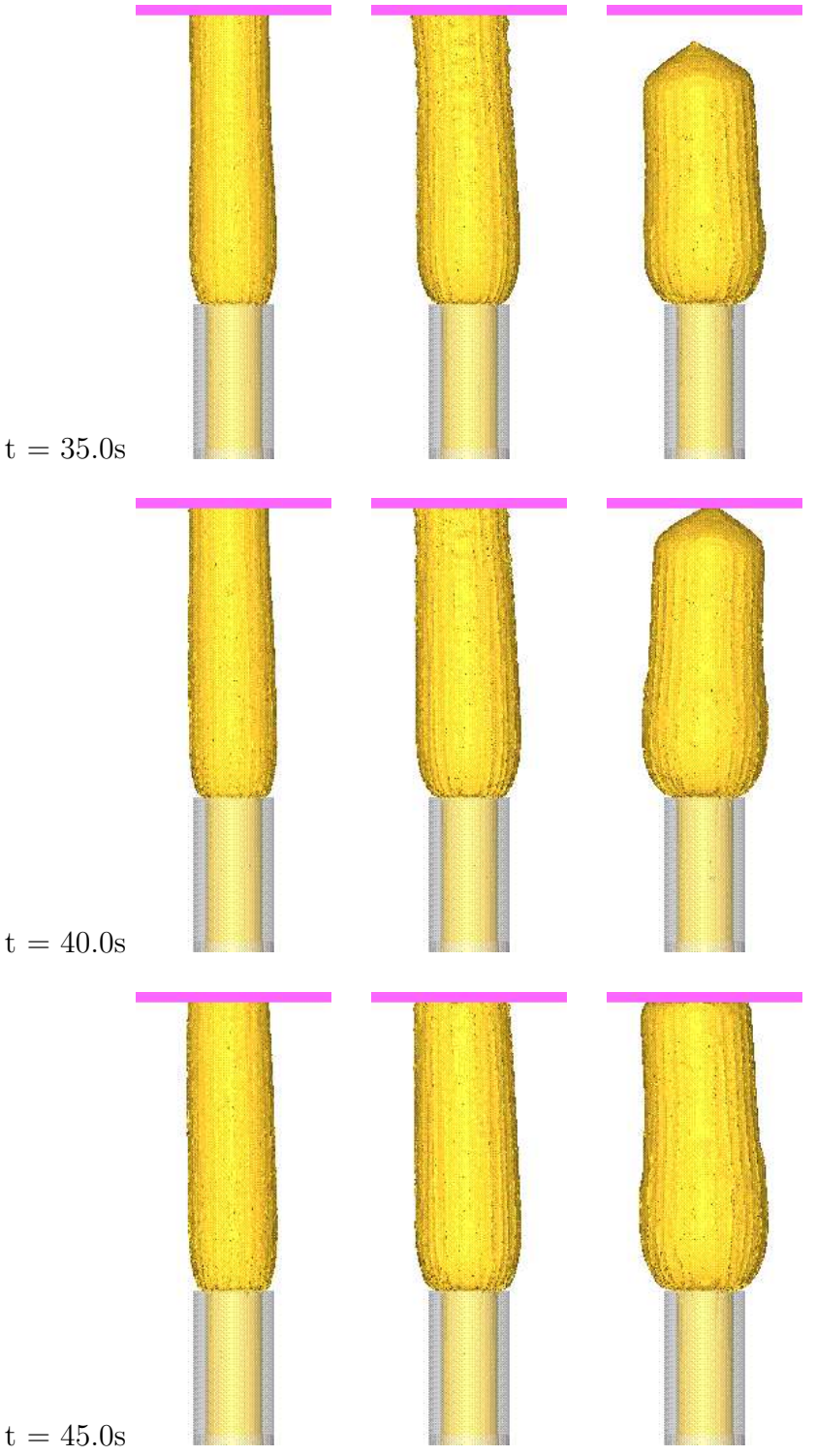


Figure 6. Continued.

Nos. 304422/2007-0, 470764/2007-4). AMA, FTP and MAA acknowledge the funding by GRICES/CAPES project number 4.1.3(CAPES/CPLP) and by FCT through projects PTDC/EQU-FTT/71800/2006, PTDC/EQU-FTT/70727/2006 and scholarship SFRH/BD/ 28828/ 2006 (AMA).

## REFERENCES

[1] V. Legat and J. -M. Marchal, Die design: an implicit formulation for the inverse problem, Int. J. Num. Meth. Fluids, 16, 29-42, (1993).

[2] M. M. Denn, Extrusion instabilities and wall slip, Annual Review of Fluid Mechanics, 33, 265-287, (2001).

[3] G. C. Georgiou, W. W. Schultz and Olson, Singular finite elements for the sudden-expansion and the die-swell problems, Int. J. Num. Meth. Fluids, 10, 357-372, (1990) .

[4] M. A. Hulsen, R. Fattal and R. Kupferman, Flow of viscoelastic fluids past a cylinder at high Weissenberg number: Stabilized simulations using matrix logarithms, J. non-Newtonian Fluid Mech., 127, 27-39, (2005) .

[5] R. G. Owens and T.N. Phillips, Computational Rheology. Imperial College Press, London (2002).

[6] R. Fattal and R. Kupferman, Constitutive laws for the matrix-logarithm the conformation tensor, J. Non- Newtonian Fluid. Mech. 123, 281-285, (2004).

[7] Y. Kwon, Finite element analysis of planar 4:1 contraction flow with the tensor logarithmic formulation of differential constitutive equations, Korea–Australia Rheol. J., 16, 183–191, (2004) .

[8] A. Afonso, O. J. Oliveira, F. T. Pinho and M. A. Alves, The log-conformation tensor approach in the finite-volume method framework, J. non-Newtonian Fluid Mech., 157, 55-65, (2009).

[9] M. F. Tomé A. Castelo, and V. G. Ferreira, S. McKee. A finite difference technique for solving the Oldroyd-B model for 3D-unsteady free surface flows, J. Non- Newtonian Fluid. Mech., 154, 179-206, (2008).

[10] D. Rajagopalan, R. Amstrong, and R. Brown. Finite element methods for calculation of steady viscoelastic flow using constitutive equations with newtonian viscosity. J. Non- Newtonian Fluid. Mech., 36, 159-192, (1990).

[11] G. K. Batchelor. *An Introduction to Fluid Dynamics*. Cambridge University Press, (1967).

[12] A. Chorin. Numerical solution of the Navier-Stokes. Maths. Comp., 2, 745-762, (1968).

[13] J.R. Clermont and M. Normandin, Numerical simulation of extrudate swell for Oldroyd-B fluid using the stream-tube analysis and a streamline approximation, J. Non-Newtonian Fluid Mech., 50, 193-215, (1993).

[14] J. I. Guermond and I. Quatapelle. On the approximation of the unsteady Navier-Stokes equations by finite element projection methods. Numer. Math., 80, 207-238, (1998).

[15] M. F. Tomé and S. McKee. GENSMAC: A computational marker-and-cell method for free surface flows in general domains. Journal of Computational Physics, 110, 171-186, (1994).

[16] M. F. Tomé, A. Castelo, J. A. Cuminato, N. Mangiavacchi, and S. McKee. GENSMAC: A numerical method for solving unsteady three-dimensional free surface flows. Int. J. Num. Meth. Fluids, 37 (7), 747-796, (2001).

[17] M. Alves, P. Oliveira, and F. Pinho. A convergent and universally bounded interpolation scheme for the treatment of advection. Int. J. Num. Methods Fluids, 41, 47-75, (2003).

[18] R. I. Tanner, A theory of die-swell, Journal of Polymer Science, 8, 2067-2078, (1970).

[19] M. J. Crochet and R. Keunings, Finite element analysis of die-swell of a highly elastic fluid, J. Non-Newtonian Fluid Mech., 10, 339-356, (1982).

[20] J. Cormenzana, A. Ledda, M. Laso and B. Debbaut, Calculation of free surface flows using CONNFESSITT, J. Rheol., 45, 237-258, (2001).

[23] V. Ngamaramvaranggul and W.F. Webster, Viscoelastic simulations of stick-slip and die-swell flows, Intern. J. Num. Meth. Fluids, 36, 539-595, (2001).

[24] A. Castelo, M.f. Tomé, C.N.L. Cesar and S. McKee, Freeflow: an Integrated simulation system for three-dimensional free surface flows, J. of Computing and Visualization in Science, 2, 199-210, (2000).